

# The Interaction Between Oxidation-Related Phenomena Along Grain Boundaries on Surface Crack Formation in Continuous Casting



GEORG GAISER , ROBERT LITTRINGER , PETER PRESOLY ,  
and CHRISTIAN BERNHARD 

Oxidation-related surface defect formation in continuous casting is an under-researched topic, as most of the experiments, which aim to define surface defect mechanisms, are performed under a protective atmosphere. However, intergranular oxidation or the formation of low-melting Cu-rich phases at the grain boundaries may lead to tremendous problems during straightening. This study exclusively addresses the impact of oxidation-related pre-defects on surface crack formation in continuous casting and how different parameters, such as cooling cycle and cooling atmosphere, affect the outcome. The investigations were performed using in-situ material characterization by bending tests (IMC-B) to evaluate crack susceptibility and simultaneous thermal analysis (STA) to analyze oxidation mechanisms in detail. Both the damage of grain boundaries by intergranular oxidation due to a low-melting fayalite-wustite eutectic and due to low-melting Cu-rich phases favor crack formation at lower temperatures significantly. A stronger external oxidation can have both positive and negative effects on surface crack formation, depending considerably on the specific steel composition. Regarding intergranular oxidation, increased external oxidation helps minimize internal and intergranular oxidation, thereby reducing potential nuclei for surface defect formation in subsequent processing steps. However, in the presence of Cu and Sn, which do not readily oxidize due to their low oxygen affinity, enhanced external oxidation promotes their enrichment, consequently increasing the risk of defect formation.

<https://doi.org/10.1007/s11663-025-03888-y>  
© The Author(s) 2025

## I. INTRODUCTION

OXIDATION processes and their influence on surface quality are an important factor in continuous casting. The slab surface temperature can reach up to 1200 °C and, depending on the cooling strategy, is exposed to varying air-mist atmospheres. Consequently, the steel surface oxidizes and scale forms. High temperatures due to hot spots (*e.g.*, surface depressions formed in the mold) accelerate these oxidation processes significantly. In addition to external oxidation, internal oxidation phenomena may form near the steel/scale interface, which are shown schematically in Figure 1.

Those internal oxidation phenomena may result in microdefects at the steel surface, affecting surface defect formation in a subsequent deformation.<sup>[1–6]</sup>

One of these phenomena is intergranular oxidation due to the selective oxidation of elements with a high oxygen affinity (*e.g.*, Si, Mn, Al). The oxidation products can be arranged near the steel/scale interface as a layer of globular oxides or as thin oxide films along grain boundaries as can be seen in Figures 1(a) and (b)). Usually, oxidation products like Al<sub>2</sub>O<sub>3</sub>, MnO, and SiO<sub>2</sub> are in a solid state. However, due to the formation of complex low-melting oxide phases they may also be in a liquid state, further enhancing internal/intergranular oxidation phenomena. Publications explicitly investigating the role of intergranular oxidation in surface defect formation during continuous casting are rare.<sup>[1–3,7]</sup> Lee *et al.*<sup>[3]</sup> demonstrated a correlation between surface crack formation and the depth of intergranular oxidation in high-Mn steel. Their results showed that deeper grain boundary oxidation increased crack formation with surface cracks forming due to the cracking of grain boundary MnAl<sub>2</sub>O<sub>4</sub>. Krobath *et al.*<sup>[1,7]</sup> and Gaiser *et al.*<sup>[2]</sup> focused on liquid-phase induced intergranular

---

GEORG GAISER, ROBERT LITTRINGER, PETER PRESOLY, and CHRISTIAN BERNHARD are with the Chair of Ferrous Metallurgy, Technical University of Leoben, Franz Josef Straße 18, 8700 Leoben, Austria. Contact e-mail: georg.gaiser@unileoben.ac.at

Manuscript submitted September 23, 2025; accepted November 16, 2025.

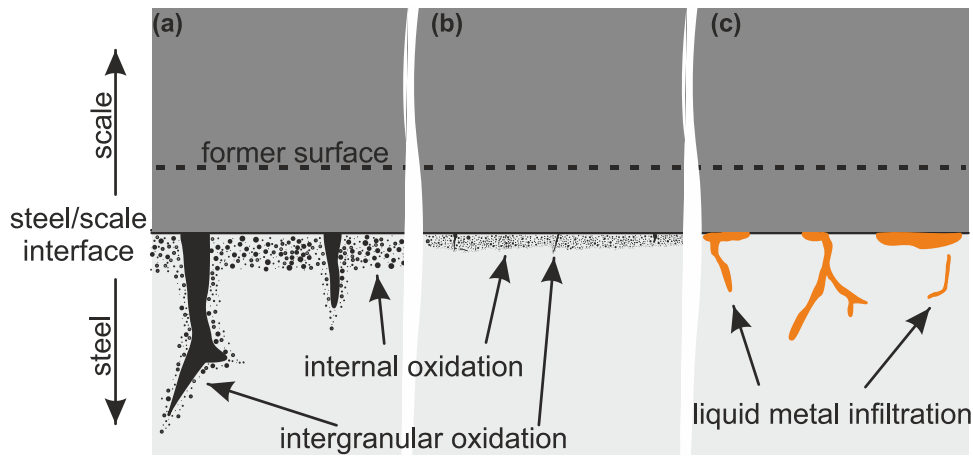


Fig. 1—Schematic representation of oxidation processes at the steel/scale interface: (a) massive intergranular oxidation due to a liquid oxide phase, (b) internal and intergranular oxidation without liquid phases, (c) formation of low-melting metal phases and liquid metal infiltration of grain boundaries.

oxidation due to a Si-rich oxide phase. Si is preferably oxidized to  $\text{SiO}_2$  and forms a low-melting eutectic compound with FeO ( $\text{FeO-Fe}_2\text{SiO}_4$ ;  $T_s \sim 1180^\circ\text{C}$ ). At sufficiently high temperatures, the liquid accumulates at the steel/scale interface and penetrates both the austenite grain boundaries, causing extensive intergranular oxidation, and the scale layer.<sup>[2,8-13]</sup> The results clearly indicate that the presence of intergranular oxidation favors surface crack formation. For a temperature with low ductility, network cracks were primarily formed at higher strain levels. Additionally, it was illustrated that grain boundary oxidation has minor influence at bending temperatures, where the ductility of the respective steel is high.<sup>[1,2,7]</sup>

A further way to form small oxidation-related surface pre-defects is the infiltration of grain boundaries due to liquid metal phases (see Figure 1(c)). The most common version is the continuous accumulation of unwanted by-elements (tramp elements) such as Cu and Sn during selective oxidation of elements with a high affinity to oxygen (Al, Si, Mn, and Fe). Regarding Cu, its solubility in austenite ranges from approximately 3 wt. pct at  $900^\circ\text{C}$  to 10 wt. pct at  $1200^\circ\text{C}$ .<sup>[14]</sup> If the solubility limit is exceeded, a separate metallic phase is formed. The presence of Sn reduces the solubility significantly and increases the amount of Cu phase formed at the steel/scale interface.<sup>[15-19]</sup> Moreover, Sn has the tendency to dissolve into the Cu phases, reducing the melting point as Cu and Sn forms a low-melting peritectic system at roughly  $800^\circ\text{C}$ .<sup>[5,19,20]</sup> During steel casting and processing, these phases are potentially in the liquid state and may penetrate the austenite grain boundaries, causing surface hot shortness in subsequent processing steps.<sup>[4,16,21-28]</sup>

The tendency for oxidation-related defect formation in the presence of Cu and Sn may be summarized by an equivalent Cu content ( $\text{Cu}_{\text{eq}}$ ).  $\text{Cu}_{\text{eq}}$  describes the content of Cu in steel, considering the interactions with other elements that increase or decrease the solubility of Cu in austenite. The most well-established ones were defined

by Wolf and Schwabe,<sup>[29]</sup> as given in Eq. [1] and Melford.<sup>[16]</sup> According to,<sup>[16,29]</sup> values of 0.25 to 0.4 wt. pct shall be considered as critical for surface defect formation. Wolf and Schwabe<sup>[29]</sup> identified Cu as the cause for the formation of fine network cracks on the strand surface and a ductility trough was presumed to be in the temperature range of  $1100$  to  $1200^\circ\text{C}$ .

$$[\text{wt.pct Cu}_{\text{eq}}] = [\text{wt.pct Cu}] + 10[\text{wt.pct Sn}] - [\text{wt.pct Ni}] - 2[\text{wt.pct S}] \quad [1]$$

However, the understanding of Cu and Sn on surface quality in continuous casting is primarily based on hot tensile tests performed under a protective atmosphere.<sup>[4,29-34]</sup> This limits their interpretability due to the unique oxidation behavior of Cu and Sn. For all those experiments, ductility was always high in the high-temperature range due to dynamic recrystallization and the proposed correlations in the  $\text{Cu}_{\text{eq}}$  (based on Eq. [1]) and the presumed critical temperature range were not clearly confirmed.

In these studies, the trough in ductility at “lower” temperatures was attributed to the formation of pro-eutectoid ferrite, the segregation of Cu and Sn toward grain boundaries and/or precipitation of fine  $\text{Cu}_2\text{S}$ .<sup>[31-33,35,36]</sup> According to Comineli *et al.*,<sup>[31,36]</sup> the interaction of (segregated) Cu with MnS seems to be the key factor. Mintz *et al.*<sup>[30]</sup> observed a similar behavior for steels with Cu, even under oxidizing conditions for both reheated and in-situ melted samples. Testing in an air atmosphere caused only a slight ductility reduction compared to a protective atmosphere, with the loss of ductility attributed to the formation of Cu-(oxy)sulfides. For the reheated samples, no influence was recognizable in an air atmosphere. Furthermore, no evidence was found that liquid Cu-rich films penetrated the austenite grain boundaries.<sup>[30]</sup>

A novelty in the field of continuous casting was presented in the works by Bernhard *et al.*<sup>[5]</sup> and Gaiser *et al.*<sup>[37]</sup> They identified a clear correlation between Cu, Sn, and Ni based on the  $\text{Cu}_{\text{eq}}$  proposed by Wolf and

Schwabe.<sup>[29]</sup> Their three-point bending experiments were performed with in-situ cast samples under oxidizing conditions in air or in an air/water vapor mixture. For 900 °C and a  $Cu_{eq}$  of roughly 0.2 wt. pct, even strains of 2 pct were enough to form the first surface cracks on the sample surface. Low-melting Cu-rich phases were clearly discernible.<sup>[5,6]</sup> Contrary to the literature, Gaiser *et al.*<sup>[6,37]</sup> further showed that steel at a temperature of 1100 °C is much more tolerant to Cu and Sn compared to 900 °C.

As mentioned at the beginning of this section, higher temperatures accelerate oxidation processes. Likewise, the oxidation atmosphere may also have a significant influence on the outcome. It is well known that the additional presence of water vapor in an oxygen, respectively, air atmosphere enhances external oxidation.<sup>[38–42]</sup> This subsequently leads to a shift in the balance between internal and external oxidation processes, whereby internal oxidation processes are normally weakened. On the other hand, increased external oxidation in the presence of accumulating tramp elements such as Cu and Sn may lead to more enrichment and a greater risk of defect formation in subsequent processes. Previous publications<sup>[2,43–46]</sup> related to oxidation experiments *via* thermogravimetric analysis have demonstrated how essential the interaction between liquid metal infiltration, respectively, internal (intergranular) and external oxidation processes, can be and how one or the other mechanism can be promoted by skillfully adjusting the oxidation parameters. However, oxidation experiments only allow an estimate and do not provide definitive information about defect formation in processes. Therefore, the direct influence of oxidation-related surface defect formation in continuous casting for different atmospheres remains practically unanswered.

Summing up, quality problems in continuous casting that specifically relate to the influence of oxidation cannot be answered in a sufficient way by applying test methods under inert conditions or singular oxidation experiments without deformation. A more refined approach to directly investigate the impact of oxidation processes on crack formation in continuous casting is the in-situ material characterization by bending test (IMC-B) developed at the Technical University of Leoben.<sup>[1,47,48]</sup> It replicates the key aspects from continuous casting such as solidification in the mold, cooling in an oxidizing atmosphere, and deformation similar to the straightening operation. The benefits of this approach were further highlighted by Lan *et al.*<sup>[49]</sup> This work specifically addresses the interplay of internal and external oxidation phenomena in an air or air/water vapor atmosphere and the extent to which it affects surface cracking for both intergranular oxidation and the infiltration of grain boundaries due to low-melting metal phases. Particular emphasis is placed on the influence of the temperature profile and the underlying oxidation atmosphere to validate how those contrasting oxidation-related defects are affected by the parameters and, consequently, their influence on surface crack formation. Within the first part of this work, a medium-carbon construction steel is investigated. Si

was used to specifically provoke the formation of intergranular oxidation and to define its role in surface crack formation. The second part of this study focuses on the same medium-carbon steel but with the addition of Cu and Sn to address the influence of low-melting metal phases on surface defect formation. Besides bending experiments *via* the IMC-B test, simultaneous thermal analysis (STA) experiments were performed to support result interpretation.

## II. EXPERIMENTAL

Table I shows the chemical composition of the two investigated steel grades and it represents the range of all investigated. P, S, and N are below 100, 40, and 80 ppm, respectively. Both steels are medium-carbon construction steels, with MC representing the base composition, while MC + Cu/Sn has slightly higher levels of Cu and Sn. MC + Cu/Sn symbolizes the expected future composition in terms of Cu and Sn and based on Eq. [1] it corresponds to a  $Cu_{eq}$  of roughly 0.25 wt. pct.

### A. In-Situ Material Characterization by Bending (IMC-B)

The IMC-B test represents a unique experimental setup for defining the susceptibility to surface crack formation in continuous casting on directly cast samples. A detailed description is given in former publications,<sup>[2,5,6,48]</sup> whereas the process and main advantages can be briefly summarized as follows:

- Every sample is prepared for casting in an induction furnace. To simulate fast solidification and cooling, as indicated by the dotted lines in Figure 2, the sample is cast in the IMC-B mold (180 mm × 58 mm × 24 mm). Both the solidification structure and the final microstructure of the sample after cooling correspond to that of the strand shell.<sup>[48,50,51]</sup>

- Cooling is performed under oxidizing conditions, representing an exclusive opportunity to assess the oxidation-related impact of intergranular oxidation and the formation of low-melting Cu-rich phases on surface crack formation on in-situ melted samples. The atmosphere can either be air or a mixture of air and water vapor.<sup>[2,5]</sup> A further option may be experiments with cooling under a protective Ar atmosphere and comparing them with an oxidizing atmosphere to further isolate the influence of oxidation and precipitation processes.

- Mechanical deformation of the sample is attained by an isothermal three-point bending procedure under conditions as close as possible to the straightening of the strand in continuous casting. The stamp velocity and displacement are the same for all experiments. Depending on the bending temperature, the maximum tensile strain values on the sample surface are up to 6.5 pct with a maximum strain rate of  $4.7 \times 10^{-4} \text{ s}^{-1}$ .<sup>[6,48]</sup> These strain rates are comparable to straightening operations in continuous casting.<sup>[52]</sup> An elasto-viscoplastic material 3D-FE model, parameterized in Abaqus, is used to calculate the stress and strain state during testing.<sup>[53]</sup>

**Table I. Chemical Composition of the Investigated Steels**

Steel	Chemical Composition [Wt. Pct]							
	C	Si	Mn	Al	Cu	Sn	Ni	Fe
MC	0.16-0.18	0.35-0.45	1.50-1.60	0.025-0.035	< 0.01	< 0.001	< 0.015	bal.
MC + Cu/Sn	0.16-0.18	0.35-0.45	1.50-1.60	0.025-0.035	0.15	0.01	< 0.007	bal.

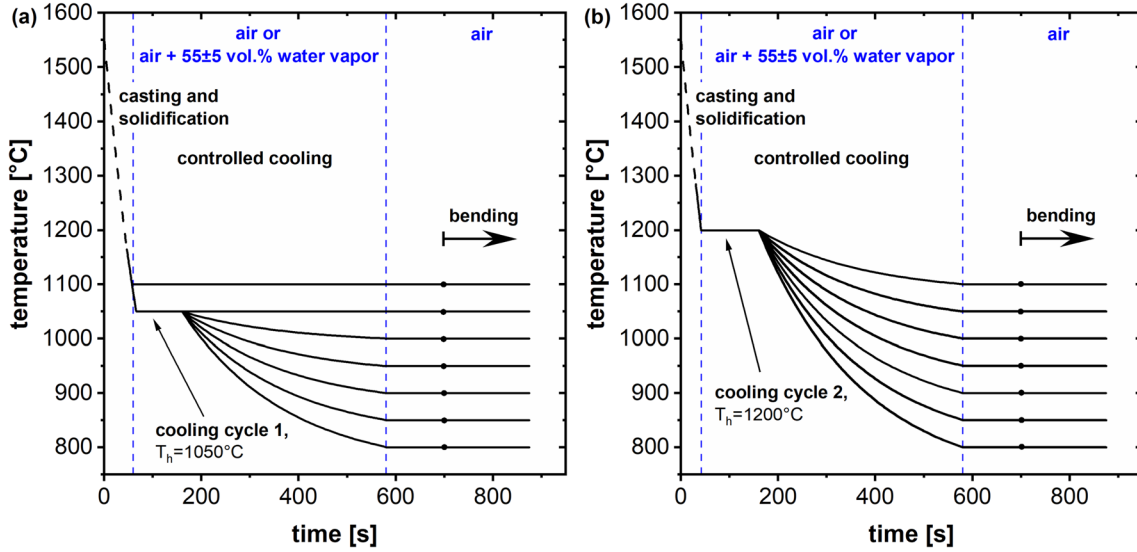


Fig. 2—Investigated cooling cycles: (a) cooling cycle 1 with  $T_h = 1050$  °C; (b) cooling cycle 2 with  $T_h = 1200$  °C.

The cooling cycles applied in this study are shown in Figure 2 and all the relevant cooling and bending parameters are summarized in Table II. The time cycles are based on a slab caster operating at a casting speed of  $1.2 \text{ m min}^{-1}$ .<sup>[47]</sup> Cooling cycle 1 represents the standard process, where the sample is stripped from the mold after 45 s at an average temperature of approximately 1180 °C. It is then cooled to 1050 °C and homogenized, resulting in a total process time of 160 s. Further cooling to the respective bending temperature continues until 580 s. Bending starts at 700 s and lasts for 175 s, with 125 s allocated for loading and 50 s for unloading. The samples for the bending temperature of 1050 and 1100 °C were held at that temperature for the complete experiment.

Cooling cycle 2 simulates extreme conditions, characterized by an elevated oxidation start temperature of about 1280 °C. This scenario represents an early detachment of the strand shell from the mold with reduced cooling in the initial phase. The sample is stripped after 30 s and homogenized at 1200 °C. Beyond this point, the time steps and bending process remain identical to those in cooling cycle 1. In both cycles, cooling up to 580 s is performed either in an air atmosphere or in an air + 55 ± 5 vol. pct water vapor mixture, while bending is always performed in air. The ambient air/water vapor mixture is set *via* humidification of dry air ( $10 \text{ l min}^{-1}$  at room temperature) by

passing it through a heated water tank (85 °C). The composition is deduced from the weight difference of the water tank before and after the experiment and the total experimental time. The parameters are set to achieve a water vapor content of roughly 55 vol. pct similar to the investigations by Wang *et al.*<sup>[54,55]</sup> and Chen *et al.*<sup>[44]</sup> The overall composition of the atmosphere is roughly 55 vol. pct  $\text{H}_2\text{O}$ , 9 vol. pct  $\text{O}_2$ , and 36 vol. pct  $\text{N}_2$ .

After bending, the samples were slowly cooled to room temperature. For investigation of oxidation phenomena, the outer part of the sample (deformation-free zone) was directly cold-embedded to protect the steel/scale interface in subsequent processing. After cutting, those samples were ground (160-320-600-800-1200) and polished (9, 3, and 1  $\mu\text{m}$ ). Detailed observations of the steel/scale interface took place *via* a digital microscope (Keyence VHX7000) and scanning electron microscope (SEM, SEM, JEOL FE-SEM 7200F) equipped with a 100 mm<sup>2</sup> SDD EDS detector (Oxford Instruments Ultim Max 100). Investigations with SEM require an appropriate conductivity of the sample, which can be ensured by sputtering the entire sample surface with a 10-nm-thin carbon layer.

Descaling of the samples was performed with diluted citric acid and the bent samples were investigated for surface defects in the strain-influenced area with a digital microscope. A schematic illustration of the sample is given in Figure 3. The crack detection

**Table II. Experimental Parameters of the IMC-B Test**

Cooling Cycle	Mold Cooling [s]	T After Mold [°C]	t After Holding [s]	t After Cooling [s]	Bending Temperatures [°C]
Cooling cycle 1	~ 45	~ 1180	160	580	800–1100
Cooling cycle 2	~ 30	~ 1280	160	580	800–1100

t Bending Start-End [s]	Maximum Strain [Pct]	Strain Rate [s <sup>-1</sup> ]	Atmosphere
700-875	5.9-6.5	$4.7 \times 10^{-4}$	air or air + 55 ± 5 vol. pct water vapor

procedure provides the total number and distribution of intergranular cracks, the critical strain  $\varepsilon_2$  for first crack formation and the crack depth.<sup>[2,5,6]</sup>

Building on previous work by the authors,<sup>[5]</sup> the determination of the critical strain based on a frequency distribution of documented cracks was further refined to capture high crack counts around the bending axis more accurately, as well as crack networks and coalescence effects of cracks. Methodologically, it is addressed as a Poisson-based system, whereas the distribution is modeled with a gaussian shaped intensity function and a hyperbolic saturation approach to account for coalescence effects.<sup>[56,57]</sup> The final distribution is optimized numerically and similar to Bernhard *et al.*,<sup>[5]</sup> the critical strain  $\varepsilon_2$  is defined as the strain value necessary to form the first 2 cracks on the sample surface based on the calculated crack distribution (see Figure 4).

### B. Simultaneous Thermal Analysis (STA)

Detailed investigations of high-temperature oxidation phenomena were performed by STA as it is an approved, quick, and easy tool for forecasting conditions in the IMC-B test.<sup>[42]</sup> The experimental setup consists of a Netzsch STA 449 F3 Jupiter equipped with a DTA-TG (Differential Thermal Analysis-Thermogravimetric Analysis) sample carrier. To maintain consistent gas conditions, the system includes high-precision pressure controllers and mass flow controllers for supplying argon, nitrogen, and synthetic air (syn. air; 80 vol. pct N<sub>2</sub>, 20 vol. pct O<sub>2</sub>). Additionally, a water vapor generator (aDrop) provides controlled humidity, while thermostats prevent condensation of the water vapor within the system. For quality control, a mass spectrometer (QMS 403 C Aeolos) monitors gas composition, and a getter furnace (Nabertherm RD30A173A) is used to enhance inert heating and cooling conditions. The getter furnace operates by passing high-purity argon (Ar 5.0, ≥ 99.999 pct purity, residual oxygen ≤ 2 ppm) through a heated tube furnace (~ 750 °C) filled with titanium granulate, effectively reducing trace oxygen levels to below 10<sup>-15</sup> ppm. To ensure performance, an oxygen-measuring device (Zirox SMG5) is used for periodic control measurements. In this study, suspended samples with a drilled hole (2.5 mm diameter) were investigated to ensure homogeneous gas flow. The samples measured 13 mm × 12.2 mm with a thickness of 2 mm. A more detailed description of the complete setup is given in former publications.<sup>[42,58]</sup>

Figure 5 illustrates the full time–temperature–gas program whereby the investigated cooling cycles represent the cooling profiles and atmosphere conditions of the IMC-B tests (see Figure 2). The cooling for a bending temperature of 900 °C is shown as an example for both cooling cycle 1 and cooling cycle 2. Heating and homogenization were always performed under a protective argon atmosphere to avoid pre-oxidation. After 15-min isothermal holding to achieve a similar grain size as in the IMC-B test, the samples were cooled to the respective stripping temperature of the IMC-B test and homogenized for a further 5 minutes. For the experiment shown in Figure 5(b), no cooling to the respective shaping temperature was necessary as the stripping temperature corresponds to the maximum furnace temperature. Afterward, cooling starts in an oxidizing atmosphere and, depending on the experiment, the oxidation atmosphere is either syn. air + 50 vol. pct water vapor and/or syn. air. The gas flow of syn. air was always 200 ml min<sup>-1</sup>. This corresponds to a gas velocity in the furnace depending on the respective oxidation temperature of up to 3.87 cm s<sup>-1</sup> (air) and 7.74 cm s<sup>-1</sup> (air + 50 vol. pct water vapor). According to a former publication, laminar flow conditions in the furnace can be assumed for all experiments.<sup>[42]</sup> Final cooling of the samples to room temperature was performed under an argon and nitrogen atmosphere to stop oxidation and to preserve the high-temperature condition. After the experiment, the samples were directly cold-embedded to protect the steel/scale interface in subsequent processing. Sample preparation and investigation are identical to the bent samples.

## III. RESULTS

### A. In-situ Material Characterization by Bending

For MC, the influence of intergranular oxidation on surface crack formation was prioritized. Cooling cycle 2 was used to specifically provoke the formation of intergranular oxidation due to the oxidation of Si and the formation of the low-melting fayalite-wustite eutectic. For MC + Cu/Sn, the focus was set on hot shortness caused by Cu and Sn, which was investigated with cooling cycle 1. The examinations and findings in this publication build upon the results of previous studies.<sup>[1,2,6,48]</sup> For a better understanding of the context of this work, those results are also presented and appropriately cited.

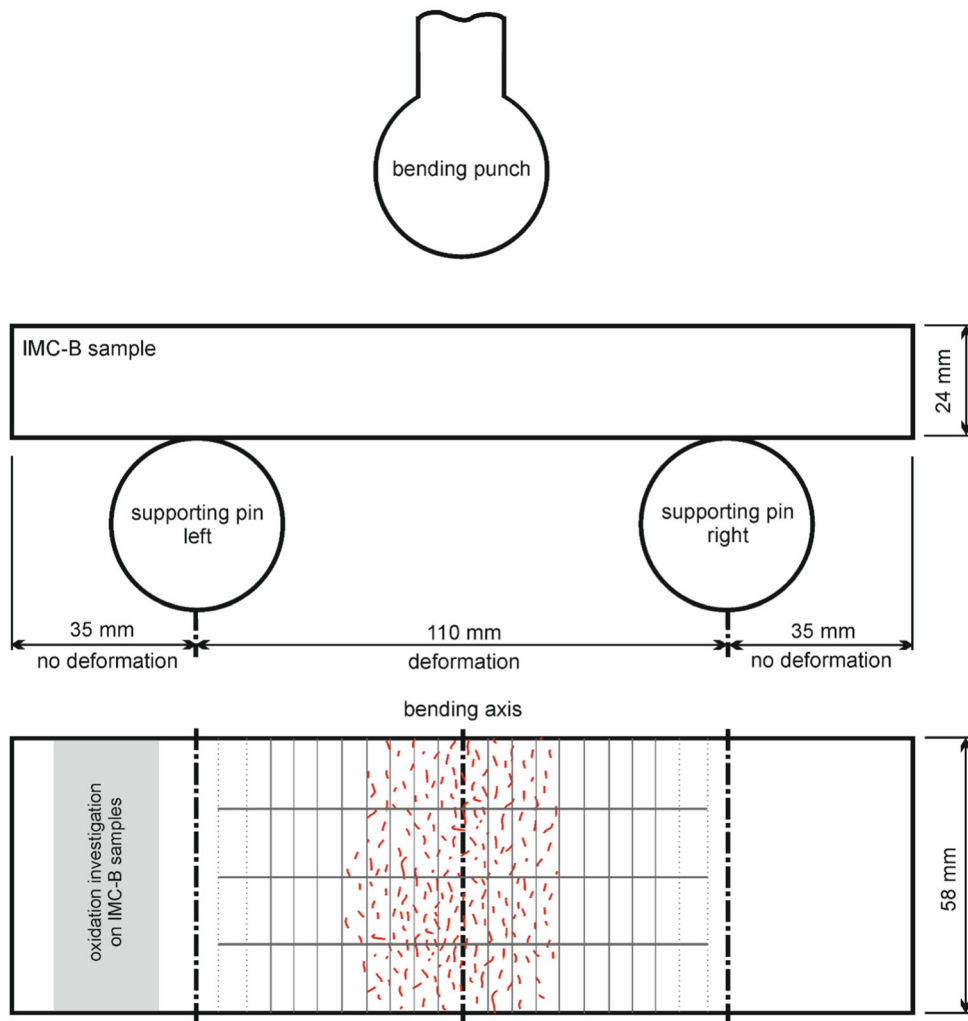


Fig. 3—Schematic illustration of the IMC-B sample.

Figure 6(a) shows the surface area around the bending axis for MC and cooling cycle 1 for both cooling in air and cooling in an air/water vapor atmosphere. Only singular cracks form and their orientation is parallel to the bending axis. The depth of the formed cracks is up to 0.5 pct (in relation to the sample thickness). The same crack appearance and maximum crack depth can be seen for cooling cycle 2, utilizing an air/water vapor cooling atmosphere. In an air atmosphere, crack formation is tremendously increased for cooling cycle 2, leading to partly formed networks and crack depths up to 1 pct (see Figure 6(b)). For MC + Cu/Sn, pronounced network cracks are preferably formed around the bending axis as it can be seen in Figure 6(c) for both cooling in air and air/water vapor. With respect to the crack depth, significant differences were observed between those two cooling atmospheres. In an air cooling, the crack depth is up to 1.2 pct, whereas in an air/water vapor atmosphere, the crack depth is up to 2 pct. For MC and MC + Cu/Sn, the average surface grain size in cooling cycle 1 is approximately 300 to 400  $\mu\text{m}$ . The influence of the bending temperature on the austenite grain size is minor.<sup>[6]</sup> For MC and cooling

cycle 2, the grain size is slightly larger and in the range of 400 to 500  $\mu\text{m}$ . The oxidation atmosphere has no influence on the surface grain size.

The results of MC in terms of the formed surface cracks are shown in Figure 7 as a clear, representative, and interpretable crack intensity map. In this evaluation, a white segment indicates a segment free of cracks, whereas yellow describes a segment with 1 to 5 cracks and red with more than 5 cracks. A hatched segment represents a very high crack number within this segment and the formation of network cracks and crack clusters. Figure 7(a) shows the crack intensity map of MC for cooling cycle 1 in an air atmosphere. Most cracks are formed at temperatures between 850 and 1000 °C in the area of the bending axis. At 800 °C, 1050 °C, and 1100 °C, the number of formed cracks is significantly reduced and more concentrated around the bending axis. Changing to cooling cycle 2 (see Figure 7(b)) leads to a tremendous increase in crack formation, especially at the temperatures 850 °C to 1050 °C. For 850 °C, 900 °C, and 950 °C, partly network cracks are formed

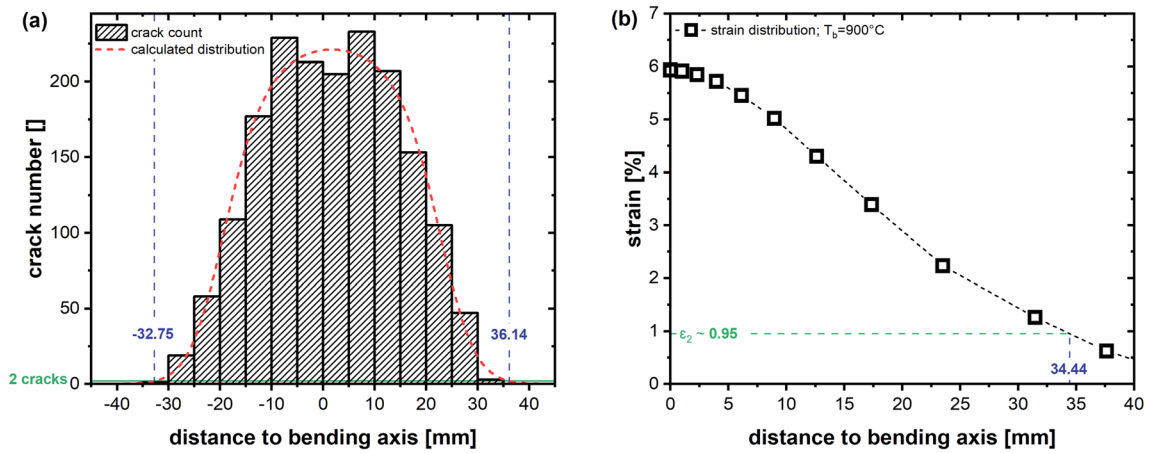


Fig. 4—(a) Number of defects per segment over the distance to the bending axis with the optimized distribution; (b) quantitative strain profile with respect to the bending axis and definition of the critical strain  $\epsilon_2$  to form 2 cracks.

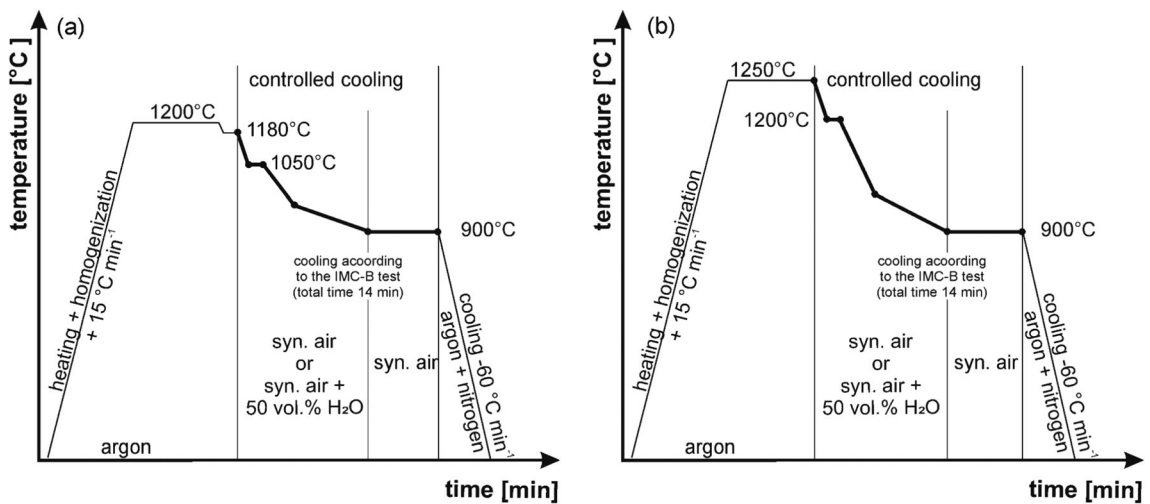


Fig. 5—Schematic illustration of the investigated STA cooling cycles: (a) cooling cycle 1 with  $T_h = 1050^\circ\text{C}$  and a simulated final temperature of  $900^\circ\text{C}$  (b) cooling cycle 2 with  $T_h = 1200^\circ\text{C}$  and a simulated final temperature of  $900^\circ\text{C}$ .

around the bending axis. At  $800^\circ\text{C}$  and  $1100^\circ\text{C}$ , the crack formation is similar to the results of cooling cycle 1.

Figure 7(c) shows the crack intensity map of MC and cooling cycle 1 in an air/water vapor atmosphere. Compared to the air cooling, the crack formation is less intense. However, the temperatures  $850^\circ\text{C}$ ,  $900^\circ\text{C}$ , and  $950^\circ\text{C}$  are clearly identifiable as the temperatures where most cracks are formed. At  $1000^\circ\text{C}$ , crack formation is noticeably reduced, whereas at  $800^\circ\text{C}$ ,  $1050^\circ\text{C}$ , and  $1100^\circ\text{C}$  hardly any cracks were formed. Utilizing an air/water vapor cooling for cooling cycle 2 (see Figure 7(d)) basically leads to the same results as for cooling cycle 1. Cracks are exclusively formed for the temperatures between  $850^\circ\text{C}$  and  $1000^\circ\text{C}$ , whereas  $800^\circ\text{C}$ ,  $1050^\circ\text{C}$ , and  $1100^\circ\text{C}$  are almost free of cracks.

Figure 8(a) compares the total number of formed cracks for MC with respect to the bending temperature for both cooling cycles and oxidation atmospheres. Irrespective of the cooling cycle, crack formation is most

intense in an air atmosphere and especially distinct for cooling cycle 2, where around 800 cracks were formed for the bending temperatures  $850^\circ\text{C}$  to  $950^\circ\text{C}$ . According to Krobath *et al.*,<sup>[1]</sup> the maximum number of cracks on the entire sample is set at 800, since a significant differentiation of individual cracks is hardly possible for numbers exceeding this limit. For cooling cycle 1, most cracks are formed at  $850^\circ\text{C}$ , counting up to 250. With increasing bending temperature, the number of formed cracks slightly decreases. At  $800^\circ\text{C}$  and  $1100^\circ\text{C}$ , hardly any cracks are formed.

In an air/water vapor atmosphere, the number of formed cracks hardly exceeds 100 cracks, irrespective of the applied cooling cycle. For cooling cycle 2 and in comparison to an air atmosphere, the number of formed cracks is reduced by approximately 90 pct. At  $800^\circ\text{C}$ ,  $1000^\circ\text{C}$ ,  $1050^\circ\text{C}$ , and  $1100^\circ\text{C}$ , hardly any cracks were formed for both cooling atmospheres.

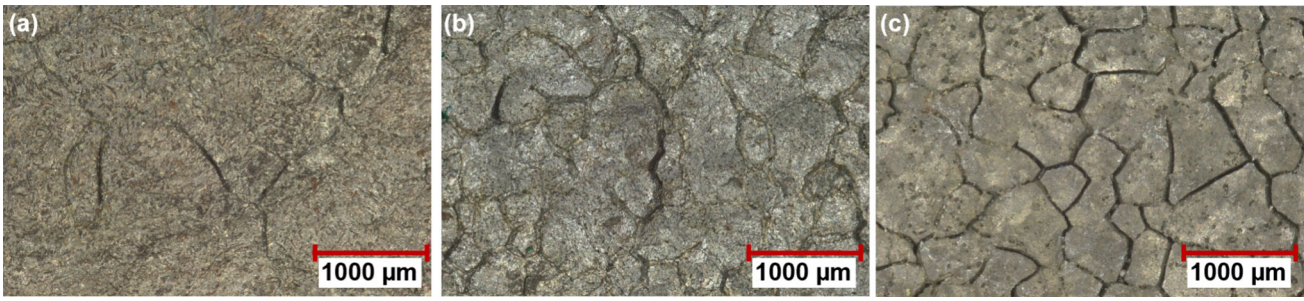


Fig. 6—Crack formation around the bending axis: (a) MC for cooling cycle 1; (b) MC for cooling cycle 2; (c) MC + Cu/Sn for cooling cycle 1.

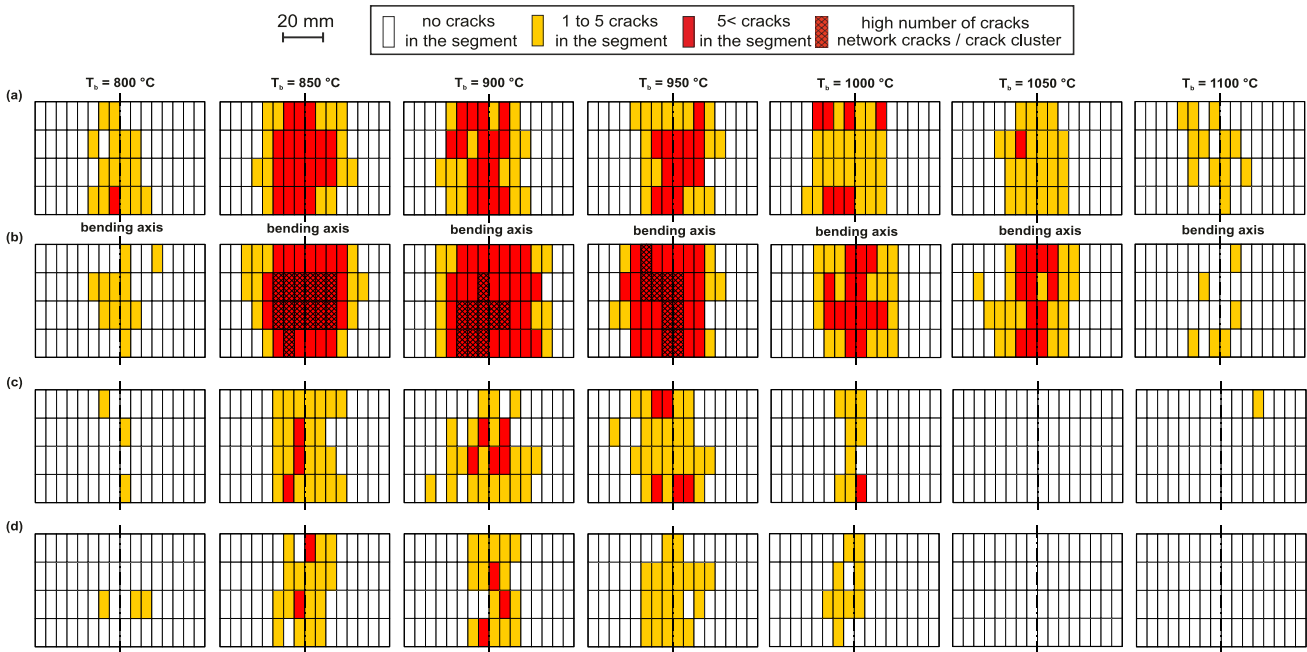


Fig. 7—Visualization of the crack intensity map for MC: (a) cooling cycle 1 in an air atmosphere (Experimental data from [48]); (b) cooling cycle 2 in an air atmosphere (Experimental data from [2]); (c) cooling cycle 1 in an air/water vapor atmosphere; (d) cooling cycle 2 in an air/water vapor atmosphere.

With respect to the critical strain for first crack formation shown in Figure 8(b), the former described relations are obvious. Within this diagram, the upper limit of mechanically induced strain for straightening in continuous casting (CC) is marked at 2 pct.<sup>[59,60]</sup> For cooling cycle 1, the lowest critical strain for first crack formation is between 2.5 and 3.5 pct in the temperature range 850 °C to 950 °C, respectively, 1000 °C in an air atmosphere. Utilizing cooling cycle 2 in an air atmosphere, the critical strain for first crack formation drops in the temperature range of 850 °C to 900 °C below the 2 pct threshold value, whereas it is roughly 2 pct at 950 °C. In an air/water vapor atmosphere, the critical strain is in the range of 4 pct or higher for the complete temperature range.

Detailed investigations from the steel/scale interface in the strain free zone show internal oxidation and pronounced intergranular oxidation for cooling cycle 2 in an air atmosphere as shown in Figure 9.<sup>[2]</sup> Based on

qualitative and quantitative analysis, the intergranular oxidation is attributed to the low-melting fayalite-wustite eutectic. Those microdefects are formed at high temperatures at the beginning of the cooling cycle but still are present at lower temperatures in the later stage of cooling. For 94 measured defects, the average depth of those microdefects is roughly 16 μm with a standard deviation of 5 μm.<sup>[2]</sup> In an air/water vapor atmosphere, no defects are observed. The same applies to cooling cycle 1 where no intergranular oxidation was observed in an air/water vapor atmosphere. The steel/scale interface is uniform, which is exhibited in Figure 10. In the air atmosphere, only two intergranular defects were observed.<sup>[2]</sup> However, due to the small sample size, no statistical significance can be determined.

Compared to MC (see Figures 7(a) and (c)), the addition of Cu and Sn (MC + Cu/Sn) significantly enhances surface crack formation as can be seen in Figure 11. The results are based on cooling cycle 1.

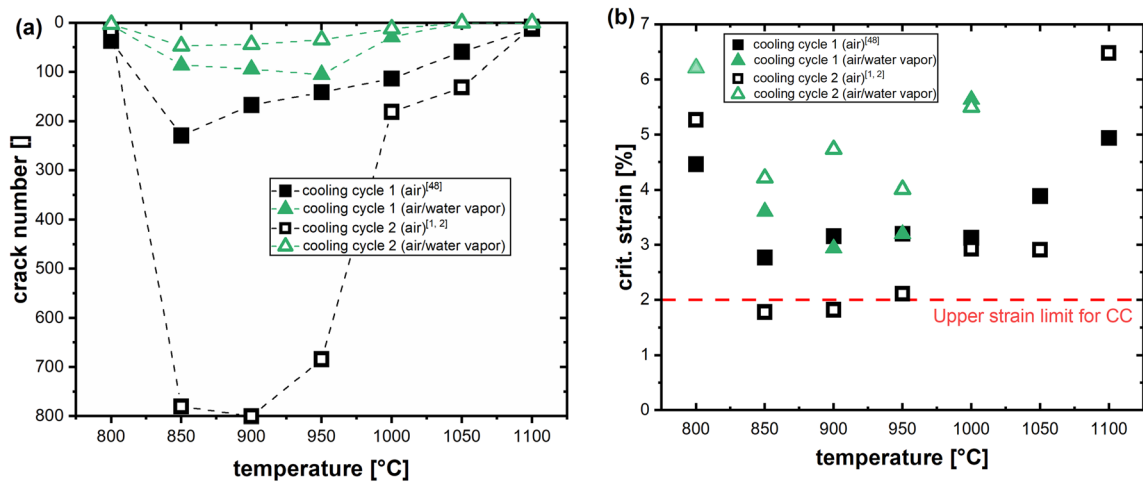


Fig. 8—Results of the IMC-B test for MC for cooling cycle 1 and 2: (a) total number of cracks vs. bending temperature; (b) critical strain vs. bending temperature..

Cooling in the air atmosphere slightly intensifies crack formation at 800 °C, whereas at 1050 °C and 1100 °C, hardly any differences to the MC grade are observed. Pronounced crack formation can be observed in the temperature range between 850 °C and 1000 °C and, in contrast to MC, crack formation is most intense at 950 °C and 1000 °C where network cracks form. The addition of water vapor in the cooling atmosphere further intensifies surface crack formation over the complete temperature range. For the temperatures 900 °C to 1050 °C, network cracks are formed around the bending axis. At 950 °C and 1000 °C, surface cracks appear almost over the entire sample surface.

The total number of formed surface cracks and the respective critical strain are shown Figures 12(a) and (b). For a better comparison, the results of MC are also visualized in those diagrams. As mentioned, the addition of Cu and Sn intensifies surface crack formation, especially in the temperature range of 950 °C and 1000 °C. In an air atmosphere, the total number of cracks is higher than 800, but to improve visualization it was capped there in the diagram following Krobath *et al.*<sup>[1]</sup> Nevertheless, at 800 °C, 1050 °C, and 1100 °C, hardly any differences can be observed in terms of formed cracks. A markedly different situation arises if the cooling is performed in an air/water vapor atmosphere. Except for 1100 °C, crack formation is significantly increased over the complete temperature range, especially distinct for 850 °C, 900 °C, and 1050 °C.

Similar trends can be observed for the critical strain. In the air atmosphere, the critical strain drops to values below 2 pct in the temperature range 900 °C to 1000 °C, especially distinct at 1000 °C, where it is below 1 pct. At 800 °C, 1050 °C, and 1100 °C, the critical strain stays well over 2 pct. The addition of water vapor in the cooling atmosphere results in a drop of the critical strain below 2 pct in a temperature range from 850 °C to 1050 °C and below 1 pct in the temperature range 900 °C to 1000 °C. Only for 800 °C and 1100 °C it stays high.

Investigations of the steel/scale interface revealed Cu-rich agglomerates at the interface and within the surface area of the steel, as can be seen in Figure 13.<sup>[6]</sup> Albeit small in size, the effect of those Cu-rich phases on surface crack formation is enormous. A more detailed view of those Cu-rich phases is given within the next chapter.

### B. Simultaneous Thermal Analysis

Detailed investigations of the appearing oxidation phenomena in the IMC-B test were performed by simultaneous thermal analysis. Figure 14 illustrates the mass gain and temperature profile of MC for both cooling cycles and cooling atmospheres and is based on Figures 5(a) and (d). Red represents cooling cycle 2 and black displays cooling cycle 1. Based on mass gain, it is obvious that the higher temperature of cooling cycle 2 leads to stronger oxidation compared to cooling cycle 1. Furthermore, it is clear that the presence of water vapor enhances oxidation, especially during cooling in the later stage of the oxidation experiment, representing lower temperatures. The overall mass gain for cooling cycle 1 is in the range of roughly 16 to 21 mg cm<sup>-2</sup>, whereas for cooling cycle 2 it is in the range of approximately 31 to 36 mg cm<sup>-2</sup>. The lower value represents cooling in an air atmosphere. Independent of the cooling cycle and cooling atmosphere, the mass gain is linear in the high-temperature region. Further cooling decreases the oxidation rate significantly, especially in the air atmosphere. Due to the earlier cooling in cooling cycle 1, the transition toward parabolic oxidation is earlier than for cooling cycle 2.

Within this diagram, a temperature of 1150 °C is marked representing the temperature where according to a former publication<sup>[43]</sup> (based on oxidation experiments) and Liu *et al.*<sup>[10]</sup> (based on Differential Scanning Calorimetry experiments), the fayalite-wustite eutectic is still liquid and may form distinct intergranular oxidation as shown in Figure 9. By comparing the mass gain

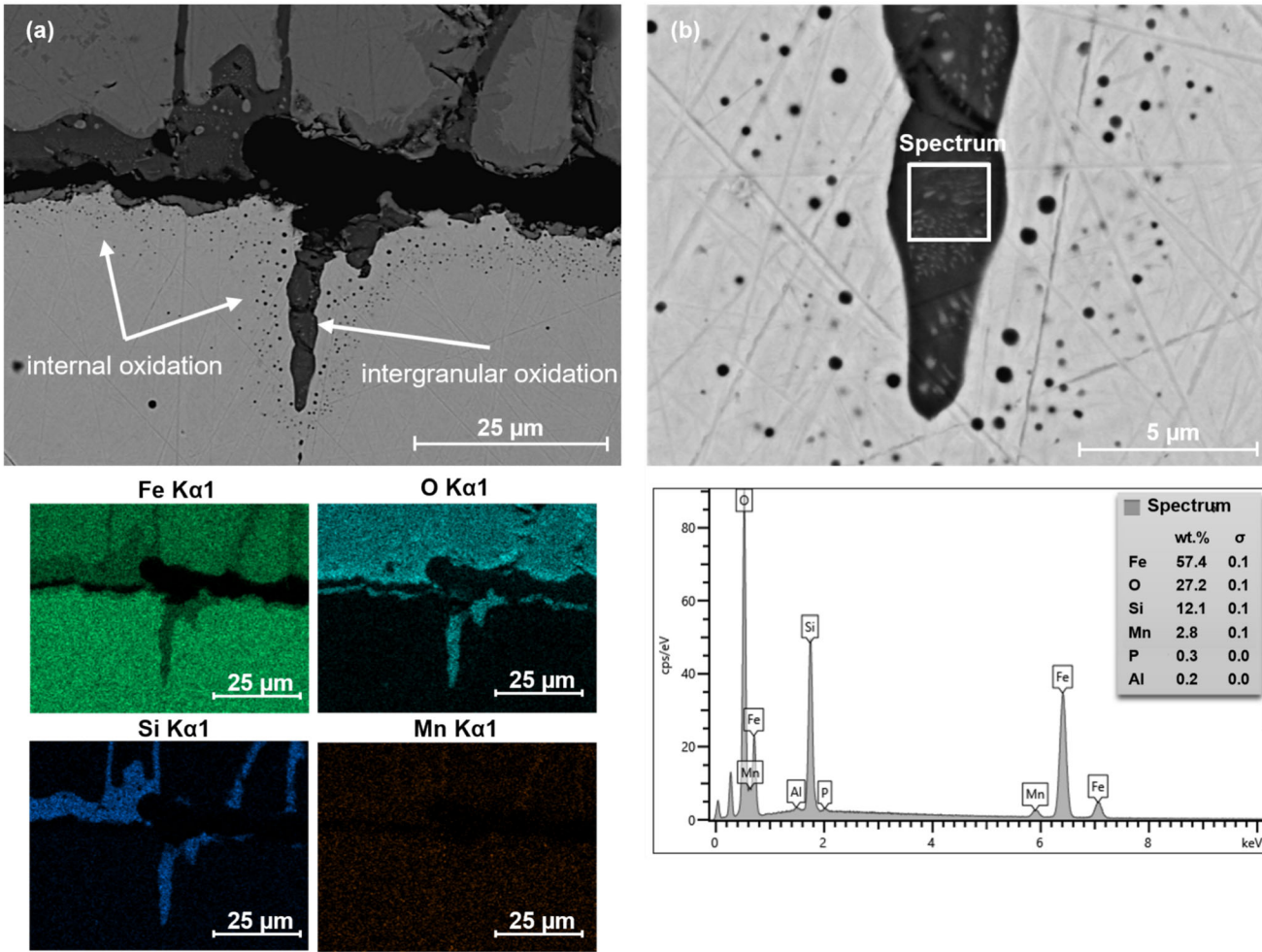


Fig. 9—(a) SEM image from the steel/scale interface of MC with qualitative element distribution for cooling cycle 1 in an air atmosphere; (b) quantitative spectrum analysis of the intergranular oxidation.<sup>[2]</sup> (Adapted under the CC-BY 4.0 license).

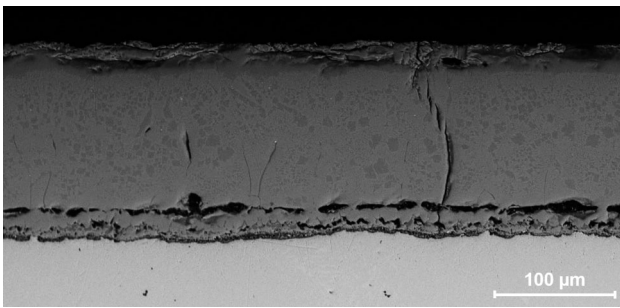


Fig. 10—Steel/scale interface of MC in an air/water vapor atmosphere.

to the point where the temperature goes below 1150 °C, using the overall mass gain it can be stated that for cooling cycle 1 in an air atmosphere roughly 50 pct of the mass gain has already occurred in the first stage where intergranular oxidation may form. For cooling cycle 2 in an air atmosphere it is even higher with approximately 90 pct. The results for cooling cycle 2

clearly indicate that the possibility of already-formed intergranular oxidation being removed due to further scaling is small. Furthermore, locally formed scale detachments are likely to happen in an air atmosphere, preserving the high-temperature condition of the interface. A metallographic cross section of such conditions is given in Figure 15. The average depth of intergranular oxidation is in the range of 18 μm with a standard deviation of 8 μm and therefore similar to the results of the IMC-B test.<sup>[2]</sup>

Differences can be seen for the air/water vapor atmosphere where the oxidation is significantly stronger in the later stage (see Figure 14). The intergranular oxidation is weakened or in the best case completely removed due to scaling. The scale layer is in contact with the steel substrate. Figures 16(a) and (b) show the condition of the steel/scale interface for both cooling cycles in an air/water vapor atmosphere. For cooling cycle 1, no intergranular oxidation was formed, whereas for cooling cycle 2 last traces of intergranular oxidation

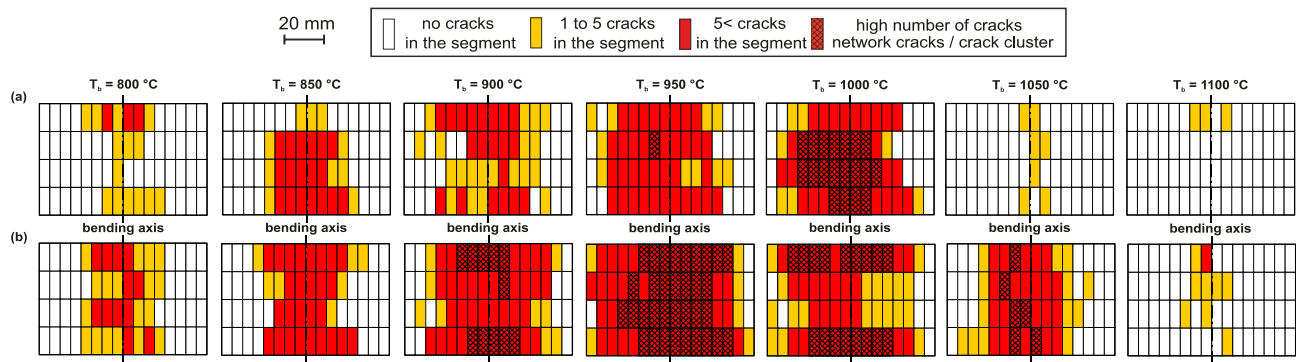


Fig. 11—Visualization of the crack intensity map for MC + Cu/Sn and cooling cycle 1: (a) air atmosphere (Experimental data from [6]); (b) air/water vapor atmosphere.

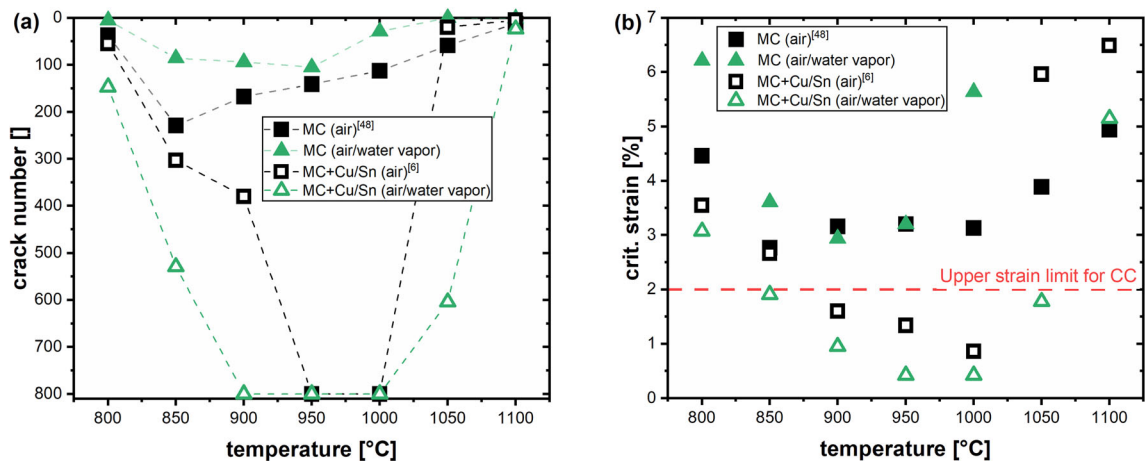


Fig. 12—Results of the IMC-B test for MC and MC + Cu/Sn for cooling cycle 1: (a) total number of cracks vs. bending temperature; (b) critical strain vs. bending temperature.

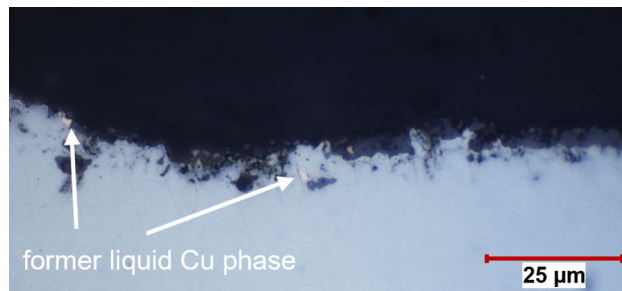


Fig. 13—Cu phases at the interface and along grain boundaries for MC + Cu/Sn at 1000 °C and cooling cycle 1. [6] (Reproduced under the CC-BY 4.0 license).

are visible. The average depth is reduced to roughly 10  $\mu\text{m}$ . Figure 16(c) shows a detail of the interface of cooling cycle 2. It is obvious that the former intergranular oxidation depth (dark gray region) is reduced due to the ongoing scaling in the later stage. The original depth is marked with red dashed lines. To further outline this mechanism, Figure 17 qualitatively illustrates the loss of intergranular oxidation depth due to scaling with quantitative area analyses.

Investigation for MC + Cu/Sn and cooling cycle 1 shows (see Figure 18) that for a bending temperature of 900 °C, the overall mass gain ranges from 18 to 23  $\text{mg cm}^{-2}$ , which is similar to MC. Increasing the final bending temperature to 1000 °C and 1100 °C rises the mass gain significantly in the presence of water vapor up to 29, respectively, 45  $\text{mg cm}^{-2}$ . However, air cooling shows only minor differences as the overall mass gain hardly exceeds 20  $\text{mg cm}^{-2}$ .

Figure 19 illustrates the steel/scale interface for all 3 investigated temperature cycles and Figure 20 presents the quantitative spectrum analysis of the Cu-rich phases. The focus is set on cooling in an air/water vapor atmosphere as those samples show no scale detachment, which may influence the interpretation. At all temperatures, the enrichment of Cu at the steel/scale interface is evident. Additionally, Cu-rich phases are clearly identifiable along surface-near grain boundaries, with higher oxidation temperatures slightly promoting their formation. Besides the Cu phases in the close vicinity of the grain boundaries at the steel/scale interface, isolated copper phases can also be seen at some distance from the surface, mostly close to oxide particles (see Figure 19(c)). An enrichment of Cu at the grain boundaries without the formation of Cu-rich phases is also

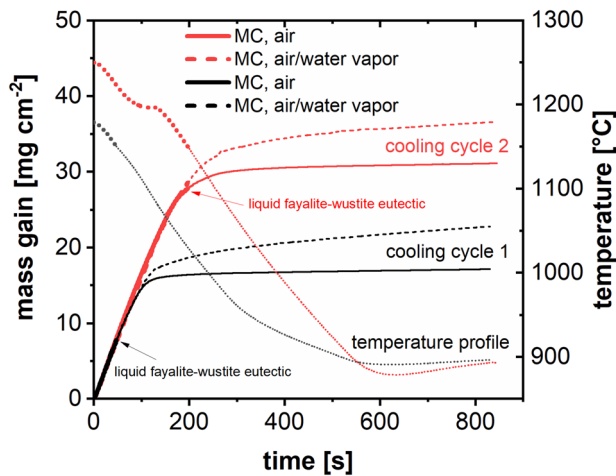


Fig. 14—Mass gain of MC for cooling cycle 1 and 2 in an air and air/water vapor atmosphere.

apparent. The composition of the Cu-rich phases can be summarized as follows: Cu concentrations range from 80 to 85 wt. pct, Sn from 6 to 9 wt. pct, Fe from 6 to 10 wt. pct, and the concentration of Ni is approximately 1 to 2 wt. pct.

#### IV. DISCUSSION

##### A. Intergranular Oxidation and Surface Crack Formation

For the investigated steel grade and cooling cycles, intergranular oxidation is attributed to the presence of the low-melting fayalite-wustite eutectic. Different cooling cycles and oxidation atmospheres lead to varying interface conditions for the subsequent bending operation. In cooling cycle 1, intergranular oxidation is hardly visible, as the stripping temperature of 1180 °C is in the range of the melting point of the low-melting eutectic in the binary FeO–SiO<sub>2</sub> system. However, based on Liu *et al.*<sup>[10]</sup> and Gaiser *et al.*,<sup>[43]</sup> the eutectic may be liquid at approximately 1150 °C, suggesting the possibility of intergranular oxidation in the initial cooling stage. Under air cooling, a few small intergranular defects were observed, but their low depth and occurrence make them statistically insignificant, so no mean value is reported in this publication. These small remnants are most likely caused by localized scale detachments, which preserve the initial high-temperature state of the steel/scale interface (as exemplified in Figure 15). In the presence of a dense scale, the oxidation medium cannot reach the sample surface and therefore the ongoing oxidation of iron involves the transport of iron cations through the scale,<sup>[61]</sup> however, they cannot diffuse across a gap, thereby maintaining the interface condition. In an air/water vapor atmosphere, no intergranular oxidation was observed.

For cooling cycle 2 under an air atmosphere, the entire austenite grain boundaries on the surface are covered with intergranular oxidation due to the high temperatures of 1200 °C or higher in the initial cooling profile. As a result, scale detachments and the generally low oxidation rate at lower temperatures preserve the high-temperature interface conditions until bending. Notable differences arise in the presence of water vapor. Water vapor is well known for enhancing external oxidation and the avoidance of scale detachments.<sup>[38–42]</sup> Consequently, as external oxidation is increased in the later stages of the experiment, where the fayalite-wustite eutectic is solid, the intergranular oxidation is gradually consumed due to scale formation (see Figures 14 and 17). Experiments using STA confirmed these trends and validated the results of the bending samples. As a result, the preservation of the high-temperature interface state is unlikely, as iron ions can continuously diffuse to the reaction zone, leading to a continuous degradation of the steel surface. In the presence of water vapor, respectively, a stronger external oxidizing environment, the balance between intergranular oxidation and external oxidation shifts more toward external oxidation. In contrast, during air cooling and the lower external oxidation, intergranular oxidation may be more dominant.

For both cooling cycles, it is obvious that the presence of air or air and water vapor hardly influences the initial linear oxidation. Therefore, it can be concluded that oxidation is mainly controlled by the presence of oxygen from the air atmosphere. Those findings are similar to the results of a former publication with isothermal oxidation experiments.<sup>[42]</sup>

In terms of surface crack formation, the differences for cooling cycle 1 between the air and air/water vapor are minor, which was expected. The critical strain for first crack formation stays similar around 3 pct and it is defined by the formation of AlN precipitates in the temperature range of 850 °C to 950 °C (1000 °C).<sup>[1,6,48]</sup> The slightly reduced crack formation for the air/water vapor atmosphere may be attributed to the fact that rare events, such as scale detachments occurring in the air atmosphere and preserving the high-temperature state of the interface, are not observed for the air/water vapor atmosphere. Therefore, there is no pre-existing intergranular oxidation that would favor the formation of surface cracks. With respect to continuous casting, such conditions can be considered uncritical. For cooling cycle 2 in an air atmosphere, the presence of intergranular oxidation significantly increases surface crack formation, particularly in a temperature range where surface ductility is already diminished. At 850 °C to 950 °C, the critical strain drops to values below 2 pct. Given that mechanical strain during straightening can reach up to 2 pct,<sup>[59,60]</sup> this presents a critical risk for surface defect formation in continuous casting. The increase in crack formation is attributed to stress concentration at microdefects during subsequent mechanical loading.<sup>[2]</sup> However, the results are strongly dependent on the cooling profile. At temperatures where surface ductility remains high, intergranular oxidation has little impact on crack formation.<sup>[1,2]</sup> In an air/water

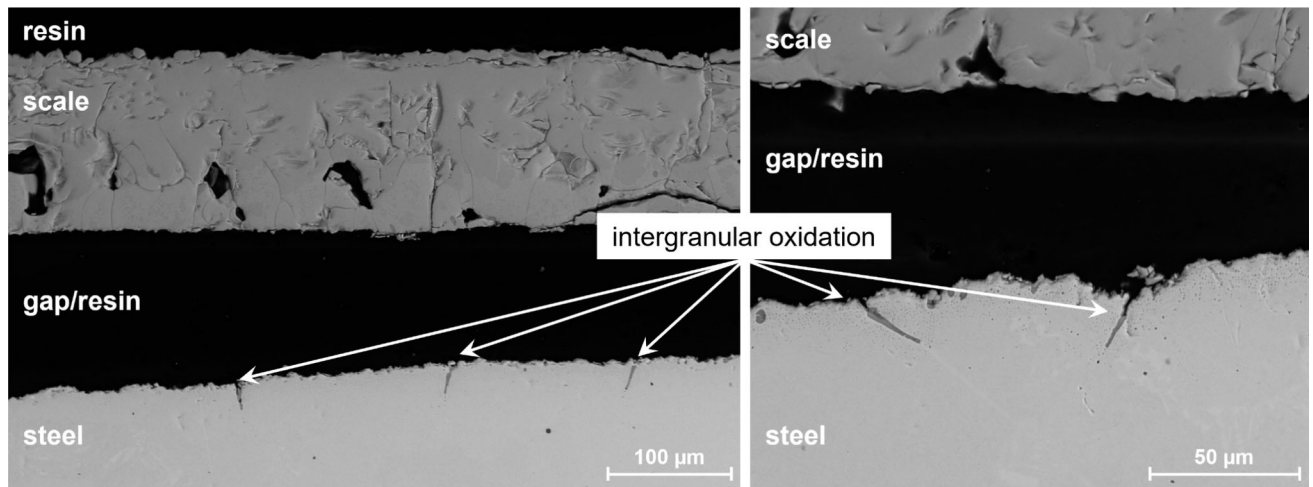


Fig. 15—Preserved high-temperature state due to a localized scale detachment for MC in an air atmosphere.

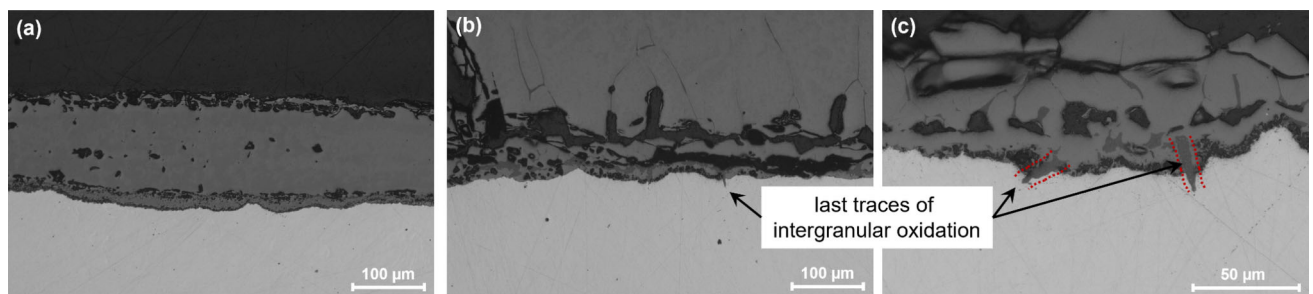


Fig. 16—Interface appearance of MC in an air/water vapor atmosphere: (a) overview for cooling cycle 1; (b) overview for cooling cycle 2; (c) detail of the interface for cooling cycle 2 with the marked original depth (red dashed lines) of the former intergranular oxidation depth.

vapor atmosphere, no increased crack formation was observed due to the absence of intergranular oxidation. In fact, crack formation was similar to that of cooling cycle 1 and even slightly reduced. Nevertheless, the temperature range of 850 °C to 950 °C remains the most critical for surface crack formation due to AlN precipitation.<sup>[1,6,48]</sup> The differences in grain size for the two cooling cycles examined are minor, which suggests that intergranular oxidation is the main influencing factor for the investigated steel grade and experimental parameters. This further highlights the crucial interplay between external oxidation and intergranular oxidation and how the oxidation atmosphere may affect crack formation.

### B. Tramp Elements and Surface Crack Formation

For all three final temperatures, the mass gain is identical at the beginning of the cooling profile until a temperature of roughly 1120 °C. At this temperature, the oxidation rate decreases noticeably in an air atmosphere, most likely attributed to scale detachments. As a consequence of the interrupted Fe ion transport path, the mass gain between 900 °C, 1000 °C, and 1100 °C remains comparable. In the presence of water vapor, external oxidation is intensified.<sup>[38–42]</sup> However, the effect depends on the temperature, as for 900 °C only minor differences may be observed between air and air water vapor. For 1000 °C, the effect of water vapor is

noticeably stronger, whereas it is most distinct at 1100 °C. This may be attributed to different aspects. Firstly, the diffusion of Fe ions through the scale is higher at elevated temperatures and secondly, the general kinetics are accelerated. Building upon the first two points, it is easier to counteract the formation of localized scale detachments at higher temperatures. Especially for 1100 °C, it can be clearly seen that the oxidation rate decreases markedly but increases again with prolonged oxidation time, which is attributed to a closed scale detachment and therefore a higher outward diffusion of Fe ions is maintained.

Due to their low affinity to oxygen, Cu and Sn enrich during oxidation along the steel/scale interface or along surfaces near grain boundaries. If the solubility limit is exceeded, a separate Cu-rich phase is formed. According to O'Neill<sup>[62]</sup> and based on the correlation between enrichment due to oxidation and back-diffusion of enriched Cu into the matrix, the temperature range between 1050 °C and 1150 °C should be considered as most critical for the formation of Cu-rich phases. Nevertheless, it strongly depends on the respective parameters. The results in this publication show that an increasing bending temperature (enhancing external oxidation) favors the formation of Cu-rich phases at the steel/scale interface. However, around surface-near grain boundaries, the differences are minor.

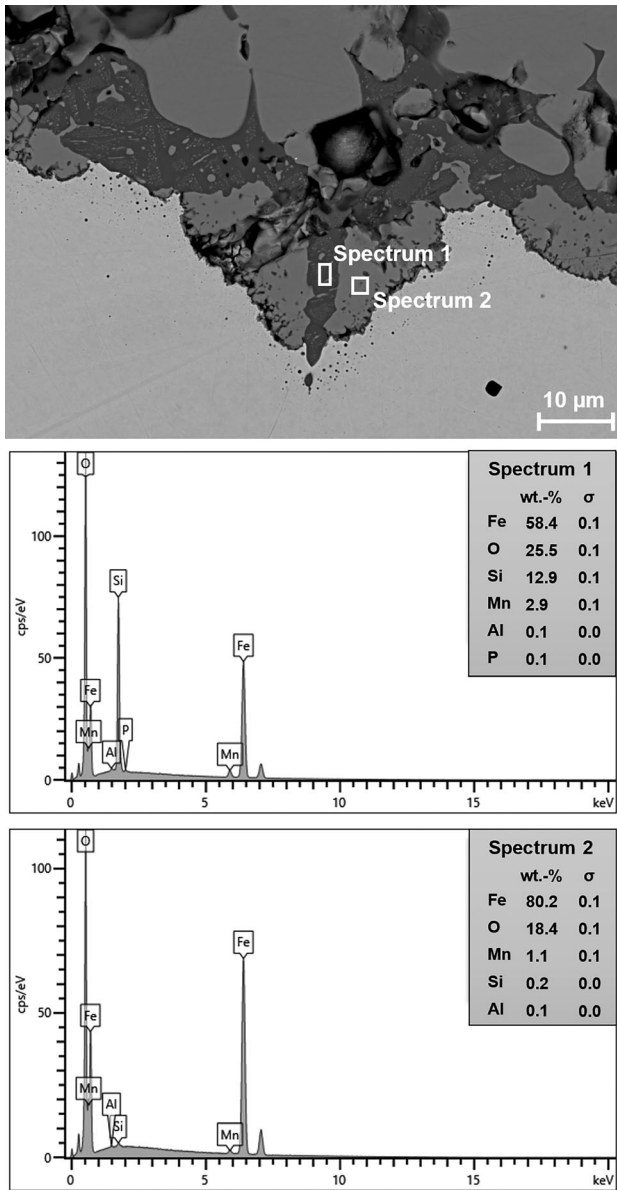


Fig. 17—Reduction of intergranular oxidation depth of MC due to scaling with chemical analysis of the appearing phases.

The concentration measurement indicates that the Cu-rich phase is enriched with Sn and Fe. Based on calculations with FactSage 8.3<sup>[63]</sup> (Database: SGTEa 2020) the solidus temperature of the measured phases (see Figure 20) is in the range of 870 °C to 900 °C, indicating that they may be most likely in (partly) liquid state during bending. Furthermore, Bernhard *et al.*<sup>[5]</sup> identified for the system 80 wt. pct Cu, 10 wt. pct Sn, and 10 wt. pct Fe *via* Differential Scanning Calorimetry and High-Temperature Laser Scanning Confocal Microscopy that the calculated solidus temperature in FactSage is ~ 30 °C higher compared to the measured ones, suggesting that at the moment the underlying database cannot replicate the reality with sufficient accuracy. This further favors the statement of partially

liquid phases at the grain boundaries during bending and provides a clear explanation for the increased crack formation in the range from 900 °C (850 °C) to 1000 °C. Since the grain size between MC and MC + Cu/Sn is practically identical, the increased defect formation is solely attributable to those phases.

Based on the results of FactSage it can be expected that for the given composition, the Cu-rich phases are in the solid state at 800 °C. Therefore, and in combination with the overall better ductility at this temperature, the crack formation is only slightly increased in relation to MC. Based on the results of the concentration measurements in this study and the findings of Bernhard *et al.*<sup>[5]</sup> regarding the accuracy of the thermodynamic database, it can be assumed that the first copper phases are partially liquid at 850 °C, thus promoting defect formation especially for the air/water vapor cooling. The improved ductility at the bending temperature of 1100 °C is likely due to a combination of factors rather than a single dominant mechanism. Firstly, the ductility of MC is generally excellent at this temperature. Secondly, at elevated temperatures, both the solubility of Cu in austenite and the back-diffusion of Cu and Sn increase.<sup>[14,15,64,65]</sup> Additionally, higher oxidation temperatures may promote the direct entrapment of Cu-rich particles within the oxide scale,<sup>[44]</sup> although this is mainly stated for temperatures in the range of 1200 °C.<sup>[19,21,22,28,44]</sup> As a result, the enrichment of Cu and Sn during oxidation, respectively, the amount of Cu-rich phases, appears to be insufficient to significantly promote crack formation at this temperature. Based on a former publication by the authors,<sup>[37]</sup> a  $Cu_{eq}$  of around 0.5 wt. pct (based on Eq. [1]) is necessary to considerably promote surface crack formation at 1100 °C. In summary, it can be concluded that the detrimental effect of low-melting Cu-rich phases is particularly severe when combined with other negative factors, such as precipitation processes (AlN for the investigated steel grades).<sup>[1,6,48]</sup> However, based on the result from MC + Cu/Sn at 1050 °C in an air/water vapor atmosphere and the results from a former publication,<sup>[37]</sup> precipitation processes do not necessarily have to occur to promote surface cracking caused by low-melting Cu-rich phases.

Comparing the results of the IMC-B test, it becomes evident that the stronger oxidation in the air/water vapor atmosphere has extended the ductility trough to lower and higher temperatures and further shifted its trend toward lower strains. Similar observations regarding oxidation and deformation have been reported by Wolf and Schwabe,<sup>[29]</sup> Kunishige *et al.*,<sup>[26]</sup> Hatano *et al.*,<sup>[66]</sup> and Shibata *et al.*<sup>[28]</sup> They identified an increased severity of cracking due to Cu-rich phases with higher water vapor content or external oxidation. Investigations by Burden *et al.*<sup>[67]</sup> indicated stronger crack formation in Cu-alloyed steel when spray water was applied to the sample surface before deformation.

Studies by Chen *et al.*<sup>[44]</sup> and Sampson *et al.*,<sup>[46]</sup> solely on oxidation experiments without any accompanying deformation, identified a positive effect of water vapor. It facilitated the entrapment of Cu-rich metal agglomerates in the scale, thereby reducing Cu-rich phases at the interface. Based on this, Sampson *et al.*<sup>[46]</sup> concluded

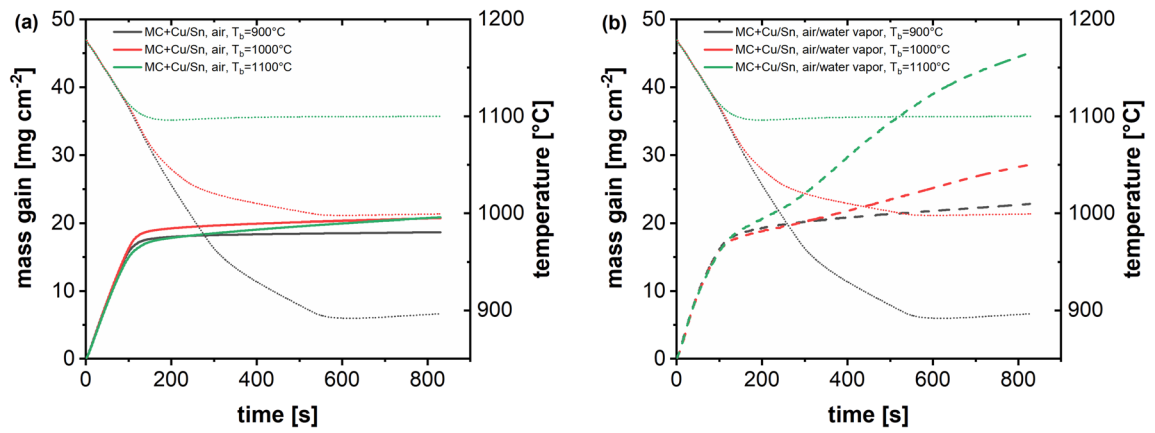


Fig. 18—Mass gain for MC + Cu/Sn and cooling cycle 1 in different cooling atmospheres: (a) air atmosphere; (b) air/water vapor atmosphere.

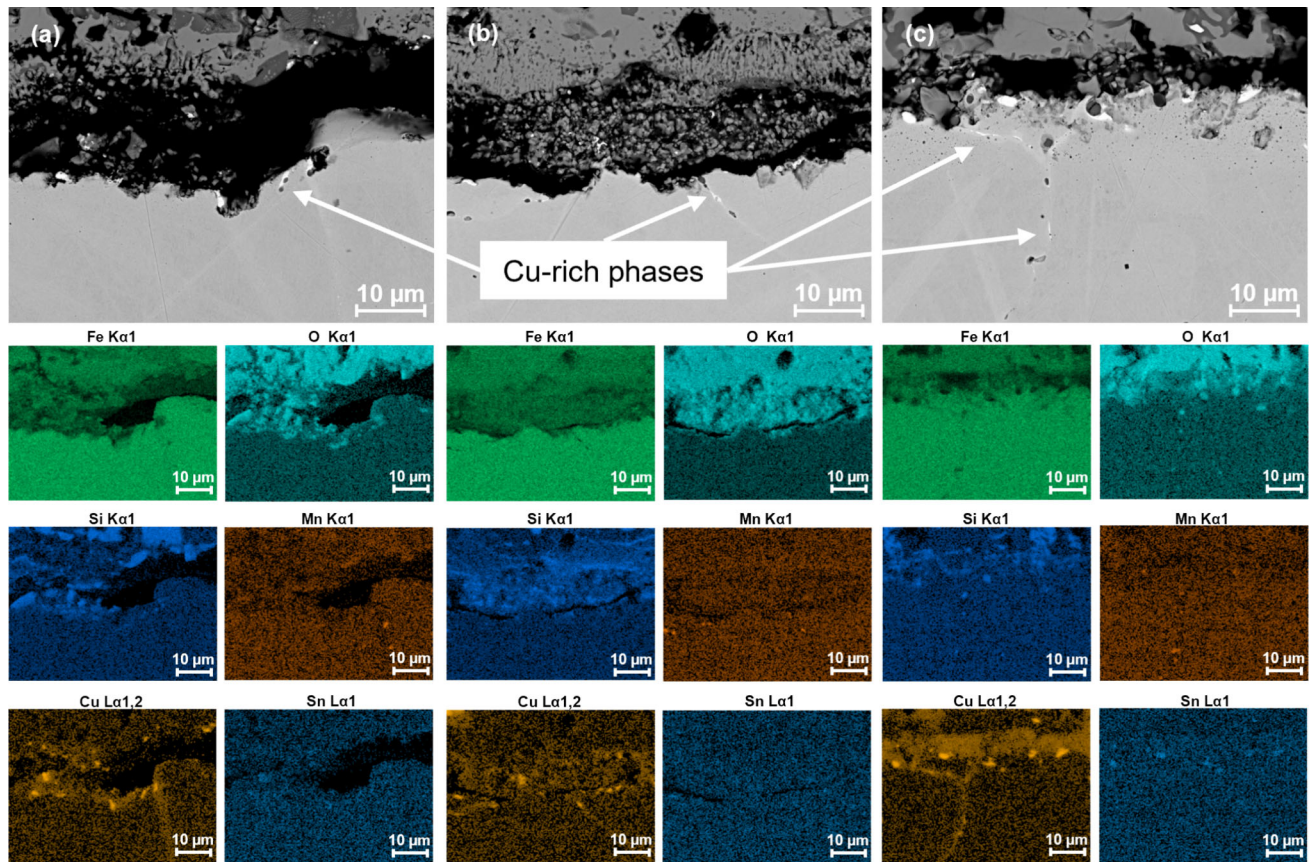


Fig. 19—Appearance of the steel/scale interface for MC + Cu/Sn for cooling in an air/water vapor atmosphere: (a)  $T_b = 900 \text{ }^\circ\text{C}$ ; (b)  $T_b = 1000 \text{ }^\circ\text{C}$ ; (c)  $T_b = 1100 \text{ }^\circ\text{C}$ .

a lower risk of hot shortness. On the other hand, Webler *et al.*<sup>[45]</sup> identified for their oxidation experiments a more pronounced penetration of Cu-rich phase along the grain boundaries in the presence of water vapor. As the oxidation kinetics between air and air/water vapor were similar for their experiments, the authors argued that this is due to the better scale adherence in the presence of water vapor and, therefore, a lower stress state at the

steel/scale interface, resulting in more favorable conditions for Cu penetration. In addition to the increased external oxidation in the presence of water vapor, and consequently the increased enrichment of Cu and Sn, the more pronounced formation of surface cracks and the higher measured crack depth compared to an air atmosphere may also be explained by the observations by Webler *et al.*<sup>[45]</sup>

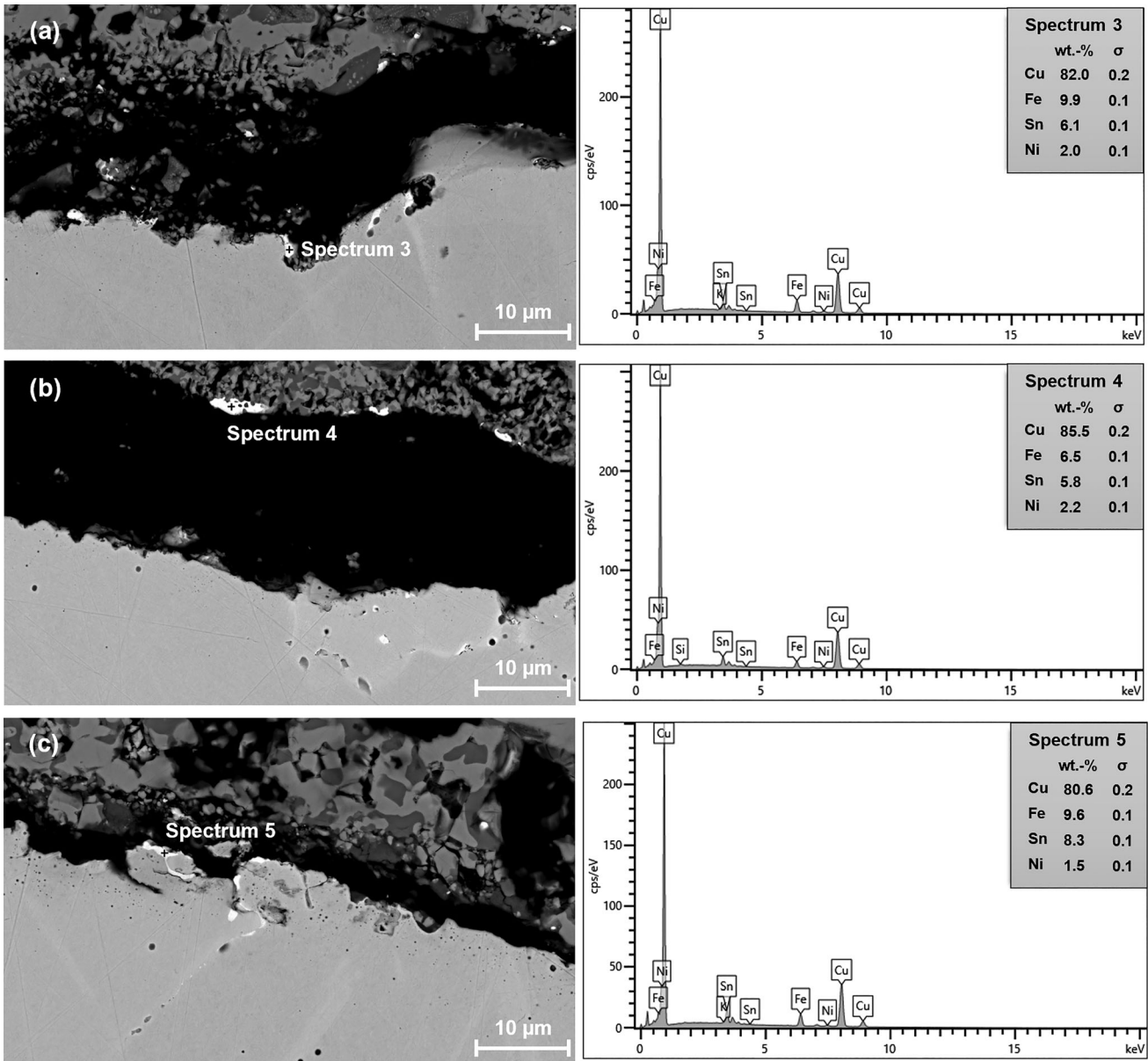


Fig. 20—Quantitative spectrum of Cu-rich phases from MC + Cu/Sn: (a)  $T_b = 900$  °C; (b)  $T_b = 1000$  °C; (c)  $T_b = 1100$  °C.

## V. CONCLUSION AND OUTLOOK

Within this publication, two different medium-carbon construction steels with and without Cu and Sn (0.15 wt. pct Cu and 0.01 wt. pct Sn) were investigated with a focus on the interplay between external and intergranular oxidation and the formation of low-melting Cu-rich phases. The investigations were performed by means of the in-situ material characterization by bending test (IMC-B) and simultaneous thermal analysis (STA). The steels were tested for different cooling cycles and atmospheres to favor different oxidation mechanisms. A dedicated focus was on the presence of water vapor in the oxidation atmosphere. The following results can be highlighted:

- If the oxidation temperature is sufficiently high, intergranular oxidation is favored due to the infiltra-

tion of austenite grain boundaries by a Si-enriched oxide phase, which can be attributed to the low-melting fayalite-wustite eutectic. Increasing external oxidation during the later cooling stage by introducing water vapor into the atmosphere leads to a significant reduction in both the depth and frequency of intergranular oxidation. The intergranular oxidation formed at high temperatures is continuously consumed by the ongoing scaling. A cooling cycle that begins near the eutectic melting point rarely leads to intergranular oxidation due to the short duration spent in the critical temperature range.

- Intergranular oxidation promotes crack formation during subsequent bending, particularly in the temperature range of 850 °C to 950 °C, where ductility is already low. These small microdefects serve as nuclei for crack growth, reducing the strain required for the

first crack formation below 2 pct. In the absence of intergranular oxidation, no increase in crack formation is observed. The presence of water vapor reduces surface crack formation compared to a pure air atmosphere and for both cooling cycles 1 and 2, the critical strain for first crack formation is in the range of 3 pct or higher.

- The presence of Cu and Sn results in an enrichment of these elements during oxidation due to their low affinity to oxygen. The ongoing enrichment during scaling favors the formation of low-melting Cu-rich phases at the steel/scale interface and at surface-near grain boundaries. From a thermodynamic perspective, these Cu-rich phases are inherently low melting.
- Surface crack formation is significantly increased in the presence of Cu and Sn. Cooling in an air atmosphere exacerbates crack formation between 850 °C and 1000 °C. The additional presence of water vapor notably broadens the ductility trough toward both lower and higher temperatures, while also reducing the strain values at which the first cracks appear. In both cooling atmospheres, the most critical temperature range for surface crack formation is between 900 °C and 1000 °C, where the critical strain is as low as 1 pct or even lower. However, at 1100 °C, minor effects of Cu and Sn on crack formation were detected. The experimental findings demonstrate that applying dry cooling in the continuous casting process (where applicable) could yield significant process benefits for steels containing Cu and Sn.
- Summing up, this study found that the presence of water vapor can have both positive and negative effects on surface crack formation in continuous casting, depending significantly on the specific steel composition. Regarding intergranular oxidation, increased external oxidation contributes to minimizing internal and intergranular oxidation processes, thereby reducing potential nuclei for surface defect formation in subsequent processing steps. However, in the presence of Cu and Sn, which are not readily oxidized due to their low affinity for oxygen, enhanced external oxidation in the presence of water vapor promotes their enrichment, consequently increasing the risk of defect formation. This investigation and its results represent a groundbreaking advancement in the field of continuous casting, as oxidation processes have largely been overlooked until now. However, the findings indicate that these processes can play a critical role in the formation of surface defects during straightening in continuous casting. Consequently, the results offer a valuable foundation for steel manufacturers and serve as a solid basis for future research in this area.

#### ACKNOWLEDGMENTS

G.G. gratefully acknowledge the funding support of K1-MET GmbH, Metallurgical Competence Center. The Research Program of the K1-MET Competence Center is supported by COMET (Competence Center

for Excellent Technologies), the Austrian Program for Competence Centers. COMET is funded by the Federal Ministry for Climate Action, Environment, Energy, Mobility, Innovation and Technology, the Federal Ministry for Labour and Economy, the Federal States of Upper Austria, Tyrol, and Styria as well as the Styrian Business Promotion Agency (SFG) and the Standortagentur Tyrol. Furthermore, Upper Austrian Research GmbH continuously supports K1-MET. R.L., P.P., and C.B. gratefully acknowledge the financial support under the scope of the COMET Program within the K2 Center 'Integrated Computational Material, Process and Product Engineering (IC-MPPE)' (Project No. 886385). This Program is supported by the Austrian Federal Ministries for Climate Action, Environment, Energy, Mobility, Innovation and Technology (BMK) and for Labour and Economy (BMAW), represented by the Austrian Research Promotion Agency (FFG), and the federal states of Styria, Upper Austria, and Tyrol.

#### FUNDING

Open access funding provided by Montanuniversitt Leoben.

#### CONFLICT OF INTEREST

The authors declare that they have no conflict of interest.

#### OPEN ACCESS

This article is licensed under a Creative Commons Attribution 4.0 International License, which permits use, sharing, adaptation, distribution and reproduction in any medium or format, as long as you give appropriate credit to the original author(s) and the source, provide a link to the Creative Commons licence, and indicate if changes were made. The images or other third party material in this article are included in the article's Creative Commons licence, unless indicated otherwise in a credit line to the material. If material is not included in the article's Creative Commons licence and your intended use is not permitted by statutory regulation or exceeds the permitted use, you will need to obtain permission directly from the copyright holder. To view a copy of this licence, visit <http://creativecommons.org/licenses/by/4.0/>.

#### REFERENCES

1. R. Krobath, C. Bernhard, S. Ilie, J. Six, S. Hahn, and P. Pennerstorfer: *BHM*, 2019, vol. 164, pp. 461–65.
2. G. Gaiser, R. Krobath, P. Presoly, and C. Bernhard: *J. Mater. Res. Technol.*, 2023, vol. 26, pp. 9276–88.
3. D. Lee, Y.-S. Kim, T.T.T. Trang, W.-T. Cho, M.-H. Kang, J.S. Lee, C.H. Yim, and Y.-U. Heo: *Eng. Fail. Anal.*, 2024, vol. 166, p. 108895.

4. M.M. Wolf: *ISIJ Int.*, 1984, vol. 24, pp. 351–58.
5. C. Bernhard, G. Gaiser, M. Bernhard, J. Winkler, M. Kern, P. Presoly, and Y.-B. Kang: *Steel Res. Int.*, 2024, vol. 27(27), p. 2400494.
6. G. Gaiser, R. Krobath, and C. Bernhard: *Metall. Mater. Trans. B*, 2025, vol. 56, pp. 4897–914.
7. R. Krobath, C. Bernhard, S. Ilie, J. Six, S. Hahn, and P. Pennerstorfer: ESTAD, European Steel Technology and Application Days, Düsseldorf, Germany, 2019.
8. L. Suarez, J. Schneider, and Y. Houbaert: *DDF*, 2008, vol. 273–276, pp. 661–66.
9. S. Taniguchi, K. Yamamoto, D. Megumi, and T. Shibata: *Mater. Sci. Eng. A*, 2001, vol. 308, pp. 250–57.
10. X. Liu, Y. He, G. Cao, T. Jia, T. Wu, and Z. Liu: *J. Iron. Steel Res. Int.*, 2015, vol. 22, pp. 238–44.
11. T. Fukagawa, H. Okada, and Y. Maehara: *ISIJ Int.*, 1994, vol. 34, pp. 906–11.
12. W. Melfo, H. Bolt, M. Rijnders, D. Staalman, C.B. Castro, D. Crowther, and B. Jana: *ISIJ Int.*, 2013, vol. 53, pp. 866–73.
13. T. Kizu, N. Yasunobu, I. Toru, and H. Yoshihiro: *ISIJ Int.*, 2002, vol. 42, pp. 206–14.
14. K. Shubhank and Y.-B. Kang: *Calphad*, 2014, vol. 45, pp. 127–37.
15. H. Ohtani, H. Suda, and K. Ishida: *ISIJ Int.*, 1997, vol. 37, pp. 207–16.
16. D.A. Melford: *Philos. Trans. R. Soc. Lond. A*, 1980, vol. 295, pp. 89–103.
17. D.A. Melford: *J. Iron Steel Inst.*, 1966, vol. 204, pp. 495–96.
18. W. Salter: *J. Iron Steel Inst.*, 1967, vol. 205, p. 1156.
19. S. Akamatsu, T. Senuma, Y. Takada, and M. Hasebe: *Mater. Sci. Technol.*, 1999, vol. 15, pp. 1301–307.
20. M. Bernhard, Y.-B. Kang, Unpublished research, 2023.
21. N. Imai, N. Komatsubara, and K. Kunishige: *ISIJ Int.*, 1997, vol. 37, pp. 217–23.
22. N. Imai, N. Komatsubara, and K. Kunishige: *ISIJ Int.*, 1997, vol. 37, pp. 224–31.
23. I. Kapoor, C. Davis, and Z. Li: *Ironmak. Steelmak.*, 2021, vol. 48, pp. 712–27.
24. I. Kapoor, C. Davis, and Z. Li: *Steel Res. Int.*, 2024, vol. 95.
25. Y.S. Lee, C.H. Jung, Y.H. Jiang, J.T. Im, Y.H. Lee, S.K. Chang, M.R. Kim, and J.H. Jun: *Mater. Sci. Forum*, 2010, vol. 654–656, pp. 386–89.
26. K. Kunishige and M. Hatano: *Mater. Sci. Forum*, 2007, vol. 539–543, pp. 4113–18.
27. Y. Kondo and H. Tanei: *ISIJ Int.*, 2015, vol. 55, pp. 1044–47.
28. K. Shibata, S.-J. Seo, M. Kaga, H. Uchino, A. Sasanuma, K. Asakura, and C. Nagasaki: *Mater. Trans.*, 2002, vol. 43, pp. 292–300.
29. M.M. Wolf and H. Schwabe: European Electric Steel Congress—Part II, Florenz, Italy, 1986.
30. B. Mintz, R. Abushosha, and D.N. Crowther: *Mater. Sci. Technol.*, 1995, vol. 11, pp. 474–81.
31. O. Comineli, A. Qaban, and B. Mintz: *Metals*, 2022, vol. 12, p. 1671.
32. H. Peng, W. Chen, L. Chen, and D. Guo: *High Temp. Mater. Process.*, 2015, vol. 34, pp. 399–405.
33. H. Matsuoka, K. Osawa, M. Ono, and M. Ohmura: *ISIJ Int.*, 1997, vol. 37, pp. 255–62.
34. C. Nagasaki and J. Kihara: *ISIJ Int.*, 1997, vol. 37, pp. 523–30.
35. N.E. Hannerz: *Trans. Iron Steel Inst. Jpn*, 1985, vol. 25, pp. 149–58.
36. O. Comineli, T. Juuti, and C. Aranas: *Steel Res. Int.*, 2017, vol. 88, p. 1600489.
37. G. Gaiser, C. Bernhard, J. Winkler, C. Lex, S. Ilie, S. Hahn, and D. Burzic: ECCC, European Continuous Casting Conference, Essen, Germany, 2024.
38. C.W. Tuck, M. Odgers, and K. Sachs: *Corros. Sci.*, 1969, vol. 9, pp. 271–85.
39. A. Rahmel and J. Tobolski: *Corros. Sci.*, 1965, vol. 5, pp. 333–46.
40. R.Y. Chen and W.Y.D. Yuen: *Oxid. Met.*, 2013, vol. 79, pp. 655–78.
41. R.Y. Chen and W.Y.D. Yuen: *Oxid. Met.*, 2013, vol. 79, pp. 679–99.
42. G. Gaiser, P. Presoly, and C. Bernhard: *Metals*, 2023, vol. 13, p. 892.
43. G. Gaiser, P. Presoly, C. Bernhard, K. Baumgartner, and S. Grosseiber: *ISIJ Int.*, 2024, vol. 64, pp. 1439–49.
44. R.Y. Chen and W.Y.D. Yuen: *ISIJ Int.*, 2005, vol. 45, pp. 807–16.
45. B.A. Weblor and S. Sridhar: *ISIJ Int.*, 2008, vol. 48, pp. 1345–53.
46. E. Sampson and S. Sridhar: *Mater. Trans. B*, 2014, vol. 45B, pp. 1769–81.
47. P. Krajewski, R. Krobath, C. Bernhard, J. Miettinen, S. Louhenkilpi, S. Ilie, and T. Schaden: *BHM*, 2015, vol. 160, pp. 109–16.
48. R. Krobath and C. Bernhard: *Steel Res. Int.*, 2020, vol. 20, p. 2000234.
49. P. Lan, Y. Lu, Y. Wang, L. Zhang, and J. Zhang: *J. Iron. Steel Res. Int.*, 2025, vol. 32, pp. 519–35.
50. H. Preßlinger, M. Mayr, E. Tragl, and C. Bernhard: *Steel Res. Int.*, 2006, vol. 77, pp. 107–15.
51. J. Reiter, C. Bernhard, and H. Presslinger: *Mater. Charact.*, 2008, vol. 59, pp. 737–46.
52. X. Zhang, H. Zhu, W. Huang, B. Shi, and A.-K. Tieu: *Int. J. Mater. Process. Technol.*, 2013, vol. 47, pp. 126–37.
53. M. Krobath, R. Krobath, C. Bernhard, and W. Ecker: *Materials*, 2020, vol. 13, p. 2281.
54. N. Wang, S. Yu, X. Li, J. Xin, G. Chen, M. Chen, and C. Huang: *J. Iron. Steel Res. Int.*, 2016, vol. 23, pp. 739–44.
55. N. Wang, J. Dong, W. Huang, B. Li, and M. Chen: *J. Iron. Steel Res. Int.*, 2014, vol. 21, pp. 1065–72.
56. A. C. Cameron and P. K. Trivedi: *Regression Analysis of Count Data*, 2<sup>nd</sup> ed., Cambridge University Press, 2014.
57. J. Illian, A. Penttinen, H. Stoyan, and D. Stoyan: *Statistical Analysis and Modelling of Spatial Point Patterns*, Wiley, 2007.
58. G. Gaiser, P. Presoly, C. Bernhard, and S. Ilie: *High Temp. Corros. Mater.*, 2025, vol. 102, p. 8.
59. B. Mintz and D.N. Crowther: *Int. Mater. Rev.*, 2010, vol. 55, pp. 168–96.
60. E.S. Szekeres: 6th International Clean Steel Conference, Balatonfured, Hungary, 2002.
61. N. Birks, G. H. Meier, and F. S. Pettit: *Introduction to the High-Temperature Oxidation of Metals*, 2<sup>nd</sup> ed., Cambridge University Press, 2006.
62. D.S. O'Neill: *PhD Dissertation*, The University of New South Wales, Sydney, 2002.
63. C.W. Bale, E. Bélisle, P. Chartrand, S.A. Decterov, G. Eriksson, A.E. Gheribi, K. Hack, I.-H. Jung, Y.-B. Kang, J. Melançon, A.D. Pelton, S. Petersen, C. Robelin, J. Sangster, P. Spencer, and M.-A. van Ende: *Calphad*, 2016, vol. 54, pp. 35–53.
64. K. Kimura, Y. Iijima, and K. Hirano: *Trans. Jpn. Inst. Met.*, 1986, Vol. 27, pp. 1–4.
65. S.K. Choudhary and A. Ghosh: *ISIJ Int.*, 2009, vol. 49, pp. 1819–27.
66. M. Hatano and K. Kunishige: *Tetsu-to-Hagane*, 2003, vol. 89, pp. 659–65.
67. M.H. Burden, G.D. Funnell, A.G. Whitaker, and J.M. Young: *Solidification and Casting of Metals*, The Metals Society, London, 1979, pp. 279–86.

**Publisher's Note** Springer Nature remains neutral with regard to jurisdictional claims in published maps and institutional affiliations.